2017

Comparison of phantom materials for use in quality assurance of microbeam radiation therapy

Matthew Cameron
University of Wollongong, mc815@uowmail.edu.au

Iwan Cornelius
University of Wollongong, iwan@uow.edu.au

Dean L. Cutajar
University of Wollongong, deanc@uow.edu.au

Jeremy A. Davis
University of Wollongong, jeremyd@uow.edu.au

Anatoly B. Rosenfeld
University of Wollongong, anatoly@uow.edu.au

See next page for additional authors

Comparison of phantom materials for use in quality assurance of microbeam radiation therapy

Abstract

Microbeam radiation therapy (MRT) is a promising radiotherapy modality that uses arrays of spatially fractionated micrometre-sized beams of synchrotron radiation to irradiate tumours. Routine dosimetry quality assurance (QA) prior to treatment is necessary to identify any changes in beam condition from the treatment plan, and is undertaken using solid homogeneous phantoms. Solid phantoms are designed for, and routinely used in, megavoltage X-ray beam radiation therapy. These solid phantoms are not necessarily designed to be water-equivalent at low X-ray energies, and therefore may not be suitable for MRT QA. This work quantitatively determines the most appropriate solid phantom to use in dosimetric MRT QA. Simulated dose profiles of various phantom materials were compared with those calculated in water under the same conditions. The phantoms under consideration were RMI457 Solid Water (Gammex-RMI, Middleton, WI, USA), Plastic Water (CIRS, Norfolk, VA, USA), Plastic Water DT (CIRS, Norfolk, VA, USA), PAGAT (CIRS, Norfolk, VA, USA), RW3 Solid Phantom (PTW Freiburg, Freiburg, Germany), PMMA, Virtual Water (Med-Cal, Verona, WI, USA) and Perspex. RMI457 Solid Water and Virtual Water were found to be the best approximations for water in MRT dosimetry (within ±3% deviation in peak and 6% in valley). RW3 and Plastic Water DT approximate the relative dose distribution in water (within ±3% deviation in the peak and 5% in the valley). PAGAT, PMMA, Perspex and Plastic Water are not recommended to be used as phantoms for MRT QA, due to dosimetric discrepancies greater than 5%.

Disciplines

Engineering | Science and Technology Studies

Publication Details

Cameron, M., Cornelius, I., Cutajar, D., Davis, J., Rosenfeld, A., Lerch, M. & Guatelli, S. (2017). Comparison of phantom materials for use in quality assurance of microbeam radiation therapy. Journal of Synchrotron Radiation, 24 (4), 866-876.

Authors

Matthew Cameron, Iwan Cornelius, Dean L. Cutajar, Jeremy A. Davis, Anatoly B. Rosenfeld, Michael L. F Lerch, and Susanna Guatelli

JOURNAL OF SYNCHROTRON RADIATION

ISSN 1600-5775

Received 4 December 2016
Accepted 13 April 2017

Edited by J. F. van der Veen

Keywords: microbeam radiation therapy; polymer phantoms; dosimetry; Monte Carlo; *Geant4*.

Comparison of phantom materials for use in quality assurance of microbeam radiation therapy

Matthew Cameron,[a] Iwan Cornelius,[b] Dean Cutajar,[a] Jeremy Davis,[a] Anatoly Rosenfeld,[a] Michael Lerch[a] and Susanna Guatelli[a]*

[a]CMRP, University of Wollongong, Wollongong, NSW 2522, Australia, and [b]Australian Synchrotron, Melbourne, VIC 3168, Australia. *Correspondence e-mail: susanna@uow.edu.au

Microbeam radiation therapy (MRT) is a promising radiotherapy modality that uses arrays of spatially fractionated micrometre-sized beams of synchrotron radiation to irradiate tumours. Routine dosimetry quality assurance (QA) prior to treatment is necessary to identify any changes in beam condition from the treatment plan, and is undertaken using solid homogeneous phantoms. Solid phantoms are designed for, and routinely used in, megavoltage X-ray beam radiation therapy. These solid phantoms are not necessarily designed to be water-equivalent at low X-ray energies, and therefore may not be suitable for MRT QA. This work quantitatively determines the most appropriate solid phantom to use in dosimetric MRT QA. Simulated dose profiles of various phantom materials were compared with those calculated in water under the same conditions. The phantoms under consideration were RMI457 Solid Water (Gammex-RMI, Middleton, WI, USA), Plastic Water (CIRS, Norfolk, VA, USA), Plastic Water DT (CIRS, Norfolk, VA, USA), PAGAT (CIRS, Norfolk, VA, USA), RW3 Solid Phantom (PTW Freiburg, Freiburg, Germany), PMMA, Virtual Water (Med-Cal, Verona, WI, USA) and Perspex. RMI457 Solid Water and Virtual Water were found to be the best approximations for water in MRT dosimetry (within ±3% deviation in peak and 6% in valley). RW3 and Plastic Water DT approximate the relative dose distribution in water (within ±3% deviation in the peak and 5% in the valley). PAGAT, PMMA, Perspex and Plastic Water are not recommended to be used as phantoms for MRT QA, due to dosimetric discrepancies greater than 5%.

1. Introduction

Microbeam radiation therapy (MRT) is a preclinical radiotherapy modality consisting of many micrometre-sized spatially fractionated radiation fields, obtained by collimating a beam of synchrotron radiation with a multi-slit collimator (Zeman *et al.*, 1959; Schültke *et al.*, 2008; Bräuer-Krisch *et al.*, 2010). A typical radiation field of MRT consists of an array of microbeams, each with a width of 50 µm and a centre-to-centre distance of 400 µm.

MRT differs from external beam radiation therapy (EBRT) due to the properties of synchrotron radiation, such as the small angular divergence of the photon beam, the broad spectrum of energies available and the pulsed high-intensity radiation that is produced (Bräuer-Krisch *et al.*, 2010). The low divergence of the beam ensures that the field does not spread out as it passes through the patient, thus maintaining the spatial fractionation at depth; the high-intensity radiation allows treatment time to be reduced, thus reducing smearing of the microbeam paths in the tissues due to breathing or cardiosynchronous motion.

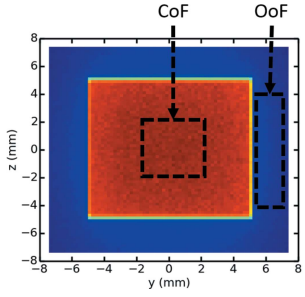

The most significant advantage of MRT over EBRT is the different radiobiological response of cancerous and healthy tissues to the micrometre-sized MRT field. As the size of the radiation field decreases to the order of micrometres the dose tolerated by normal tissue increases dramatically, whilst maintaining tumour control (Zeman *et al.*, 1959; Bräuer-Krisch *et al.*, 2010). This phenomenon, called the dose-volume effect, makes MRT a promising treatment for radioresistant tumours such as osteosarcomas, or tumours located within or near sensitive structures (*e.g.* glioblastomas in paediatric patients).

The dose tolerance of normal tissue remains the limiting factor in the delivery of dose using MRT. The peak-to-valley dose ratio (PVDR) (Siegbahn *et al.*, 2006) is an important dosimetric quantity for MRT that determines the effectiveness of the treatment. A high PVDR means that greater peak doses can be delivered for the same valley dose which, along with the out-of-field dose caused by scattering, must be well below normal tissue tolerance for an acceptable patient clinical outcome (Rothkamm *et al.*, 2012).

MRT is still in the pre-clinical stage, and more research is needed before progressing to clinical trials. The ID17 biomedical beamline of the European Synchrotron Radiation Facility (ESRF, Grenoble, France) has developed the world's first MRT facility capable of routine irradiation of tumour-bearing rodents. A treatment planning system has been developed for preclinical trials (Bartzsch, 2011; Debus, 2012), irradiation of implanted tumors in rodents is ongoing (Fernandez-Palomo *et al.*, 2015), and pet animal patient trials on pets such as cats and dogs have commenced recently (Bravin *et al.*, 2015).

Effective quality assurance (QA) for MRT is necessary to mitigate the risk of delivering an incorrect dose to the patient (Ortiz *et al.*, 2009). Because of the complex system of radiation field delivery, it is crucial to establish a QA procedure to predict the dose delivered to the patient very accurately.

The IAEA TRS-398 code of practice recommends that dosimetric QA be based on a standard of absorbed dose to water (Andreo *et al.*, 2000). The recommendation is to perform relative dose measurements in a water tank phantom as water is considered the best widely available alternative to soft tissue for most energies (Svensson *et al.*, 1994). This is due to the fact that the human body is largely water, thus absorption and scatter properties are very similar.

Unfortunately, water tank phantoms can be inconvenient to set up correctly due to time required for filling, positioning and draining, and so are generally used for quarterly or annual QA tests. Additionally, few commercial waterproof dosimeters are available for high-spatial-resolution dosimetry at the micrometre scale as applicable to synchrotron radiation. Radiochromic film is capable of resolving dose at the necessary spatial resolution, but is hampered by a long development time (Crosbie *et al.*, 2008). The PTW microDiamond detector is capable of real-time dosimetry of synchrotron microbeams, but set-up requires a lengthy and difficult alignment process to avoid geometric effects degrading spatial resolution (Livingston *et al.*, 2016). Unique silicon single strip detectors, which are specially packed in a kapton pigtail used for MRT real-time dosimetry (Rosenfeld *et al.*, 2005; Petasecca *et al.*, 2012; Lerch *et al.*, 2011, 2017), have been used in water but have not been specifically designed for that.

The small radiation field (with field sizes of 10 mm × 10 mm as opposed to 10 cm × 10 cm for EBRT) and the delivery of micrometre-sized photon beams can have an impact on the scattering properties of the radiation field in the phantom. Siegbahn *et al.* (2006) state that photon scattering is mostly responsible for dose in the middle of the valley and electron scattering contributes mostly to dose closer to the peak (De Felici *et al.*, 2005). Others have noted preferential out-of-field scatter due to the polarization of the synchrotron radiation (Bartzsch *et al.*, 2014) which influences the valley dose and out-of-field dose. The dose in these areas is a limiting factor for treatment as it must be kept below normal tissue tolerance and thus must be accurately known for effective QA and treatment.

An alternative to water tank phantoms is the use of water-equivalent solid phantoms, which are preferred for routine QA to verify the correct beam properties prior to treatment due to ease of use and speed of measurement. However, the different composition of the solid phantoms means that the absorption and scattering properties may not match those of water. Hugtenburg *et al.* (2010) suggest that the dosimetric accuracy should be within 5% for a successful clinical outcome whereas the IAEA (Andreo *et al.*, 2004) recommends an accuracy of 3% and ICRU Report 44 recommends that correction factors are required if uncertainties are greater than 1% (ICRU, 1989).

Owing to the inherent difficulty of dosimetry of such small radiation fields, uncertainties of up to or even greater than 10% may be considered 'acceptable' during this preclinical stage depending on the decision of the individual. A reference acceptable limit of relative dosimetric differences between solid and water phantoms for MRT QA is yet to be agreed upon. This is an important issue, which is one of the goals of the Dosimetry and Treatment Planning Working Group of the SYRA3 COST action (https://www.syra3.eu/). Recently, Fournier *et al.* (2016) published a paper outlining a standard method for dosimetry of MRT using a PinPoint ion chamber, and provides an uncertainty of ion chamber measurements of 4.4%.

Hill *et al.* (2010, 2014) have shown that phantom materials may not be water-equivalent (and thus tissue-equivalent) in the low-energy X-ray region. This was tested for a number of phantom materials at energies between 50 kVp (approximate mean energy 17 keV, approximate maximum energy 50 keV) and 280 kVp (approximate mean energy 93 keV, approximate maximum energy 280 keV). The radiological water equivalence of commonly used solid phantoms has never been studied for a synchrotron beam.

Since solid phantoms are the most widely used for daily QA in clinical practice, it is vital to study which phantom materials are suitable for absolute and relative dosimetry for MRT QA.

This project investigates the suitability of different solid phantoms commercially available for MRT by means of

Monte Carlo simulations. The phantoms under study were: RMI457 Solid Water (Gammex-RMI, Middleton, WI, USA), Plastic Water (CIRS, Norfolk, VA, USA), Plastic Water DT (CIRS, Norfolk, VA, USA), PAGAT (Computerized Imaging Reference Systems), RW3 Solid Phantom (PTW Freiburg, Freiburg, Germany), PMMA from Virtual Water (Med-Cal, Verona, WI, USA) and Perspex.

Previous studies have determined the radiological water equivalence of phantoms in low-energy X-ray beams in conventional kilovoltage X-ray radiotherapy (Hill *et al.*, 2010, 2014). Our study focuses on studying the applicability of these phantom materials in typical photon spectra used in MRT.

2. Method

2.1. Comparison of phantom mass energy-absorption coefficients

Radiological water-equivalence of homogeneous phantoms is determined by how well the attenuation and scattering properties of the material agree with those of water. Given the dependence of the attenuation coefficient on the incident photon energy, which has direct correlation to the theoretical calculation of water equivalence, it is necessary to know the energy spectrum in detail. Thus, provided good characterization of the energy spectrum of the radiation field that will interact with the material, a theoretical estimate of radiological water-equivalence can be obtained. The energy spectrum of the incident radiation field used in this paper is derived from Cornelius *et al.* (2014) which models, using *Geant4*, the geometry of the ESRF ID17 biomedical beamline and is already well matched to experimental results (see Fig. 1). Photon energies range approximately between 20 keV and 300 keV, with an average energy of 100 keV as calculated from the spectrum of X-rays at the entrance to the phantom.

The mass energy-absorption coefficients μ_{en}/ρ of the alternative phantom materials were calculated to provide a first measure of radiological water equivalence, as done by Brown *et al.* (2008). Then the work was refined by studying the radiological water-equivalence of the solid phantoms by means of Monte Carlo simulations as they provide an accurate description of the beam geometry, attenuation and scattering of the polarized photon beam, detailed transport of secondary electrons, and calculation of the dose at the micrometre scale, which is required by MRT-related studies.

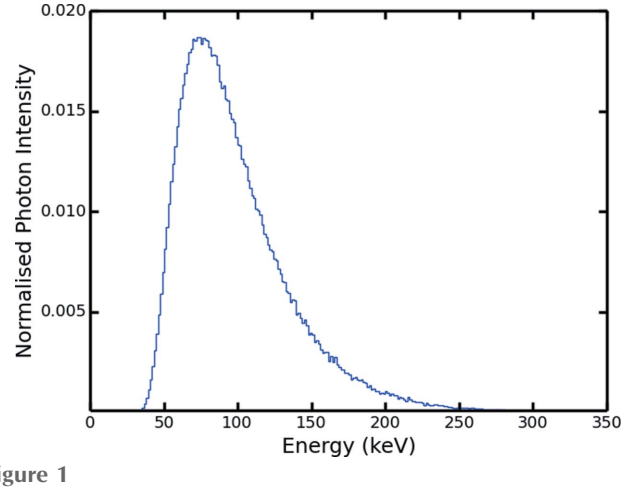

Figure 1
Energy spectrum of the synchrotron radiation produced by the ESRF biomedical beamline ID17 wiggler incident on the phantom, calculated by Cornelius *et al.* (2014).

The mass energy-absorption coefficients of the phantom materials under study were approximated using a fraction-by-weight formula from the mass energy-absorption coefficients of the component elements of the investigated material. This approximation is known to underestimate the true mass energy-absorption coefficient of the composite material by up to 5% for mixtures of high- and low-Z and high photon energies (Attix, 1984) but will suffice for this preliminary study. Elemental mass energy-absorption coefficients were taken from Hubbell & Seltzer (1993) and mass energy-absorption coefficients of the composite materials were calculated as follows,

$$\left(\frac{\bar{\mu}_{en}}{\rho}\right)_{compound} = \sum_{i=1}^{n} w_i \left(\frac{\bar{\mu}_{en}}{\rho}\right)_i, \qquad (1)$$

where n is the number of elements in the material, i is the index of the element to be summed, and w_i is the fraction by weight of the ith element in the compound.

The percentage difference of mass energy-absorption coefficient $\Delta(\bar{\mu}_{en}/\rho)$ for a given solid phantom (p) to water (w) was calculated as follows,

$$\Delta(\bar{\mu}_{en}/\rho) = \frac{(\bar{\mu}_{en}/\rho)_p - (\bar{\mu}_{en}/\rho)_w}{(\bar{\mu}_{en}/\rho)_w} \times 100. \qquad (2)$$

2.2. The *Geant4* simulation application

The study was performed with the *Geant4*-based application modelling the ESRF ID17 biomedical beamline (Grenoble, France), described by Cornelius *et al.* (2014). *Geant4* is a Monte Carlo (MC) simulation toolkit modelling the interactions of particles with matter (Agostinelli *et al.*, 2003; Allison *et al.*, 2006, 2016). The *Geant4* version used in this project was 4.9.6, patch 02.

The *SHADOW* code (Sanchez del Rio *et al.*, 2011) was adopted to model the synchrotron X-ray production in the ID17 wiggler. The photons were then transported through the ID17 beamline, including the ionization chambers, filters, multi-slit collimator (MSC) and a 20 cm × 30 cm × 30 cm homogeneous solid phantom of the material under examination, as described by Cornelius *et al.* (2014). A simplified diagram of part of the geometry and the coordinate system used in the simulation experimental set-up is shown in Fig. 2.

The different phantom materials under study were modelled in the *Geant4* simulation. The material characteristics (density and chemical composition) of all materials except Perspex were obtained from Hill *et al.* (2008). However, in the cases of Plastic Water, Plastic Water DT,

Table 1
Material composition of phantom materials under investigation.

	Material fraction by weight								
Element	Water	RM1457 Solid Water	Plastic Water	RW3 Solid Phantom	Perspex	Virtual Water	Plastic Water DT	PAGAT	PMMA
H	0.1119	0.0809	0.0925	0.0759	0.0805	0.0770	0.074	0.1059	0.0805
B	–	–	–	–	–	–	0.0226	–	–
C	–	0.6722	0.6287	0.9041	0.5998	0.6873	0.4674	0.0681	0.5999
N	–	0.024	0.01	–	–	0.0227	0.0156	0.0242	–
O	0.8881	0.1984	0.1794	0.008	0.3196	0.1886	0.3352	0.8014	0.3196
F	–	–	–	–	–	–	–	–	–
Mg	–	–	–	–	–	–	0.0688	–	–
Al	–	–	–	–	–	–	0.014	–	–
P	–	–	–	–	–	–	–	0.0002	–
Cl	–	0.0013	0.0096	–	–	0.0013	0.0024	0.0002	–
Ca	–	0.0232	0.0795	–	–	0.0231	–	–	–
Br	–	–	0.0003	–	–	–	–	–	–
Ti	–	–	–	0.012	–	–	–	–	–
Density (g cm^{-3})	1	1.03	1.013	1.045	1.19	1.03	1.039	1.026	1.18

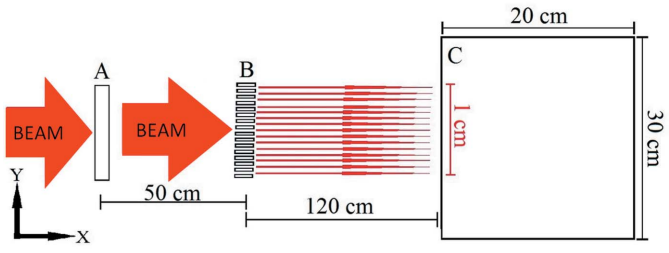

Figure 2
Setup of the *Geant4* simulation showing: A, vertical slit; B, MSC; C, phantom (not to scale). The z direction is orthogonally up out of the page.

Virtual Water and PAGAT the total fractional weights were not equal to unity and thus the element with the largest fractional weight was increased slightly ($\leq$0.0005) to achieve unity. The chosen element in PAGAT was oxygen and in all other cases the chosen element was carbon.

The material characteristics of Perspex were taken from NIST (Berger *et al.*, 1998). Table 1 reports the chemical composition and the density of the phantom materials under study. It should be noted that exact material characteristics of solid phantoms in reality vary depending on many factors during the manufacturing process.

Two beam configurations were simulated in order to investigate the effect of the phantom material on dose distribution. The first configuration under study (henceforth called *broad-beam configuration*) produces a broad field by scanning the phantom through a 10 mm (y direction) $\times$ 0.5 mm (z direction) beam without the MSC in place. Broad-beam is used to examine dose distribution in a non-collimated synchrotron radiation field in order to establish trends of the material responses and provide a comparison point for previous small-field low-energy EBRT results.

The second configuration under study (henceforth called *microbeam configuration*) was selected to determine the effect of the phantom material on the microbeam dose distribution. To achieve this goal, the MSC was placed in the synchrotron beam to produce 125 microbeams, each with a width of 50 µm, 500 µm height and pitch of 400 µm.

The low-energy Livermore polarized physics package (Chauvie *et al.*, 2004) was adopted to model the electromagnetic interactions of particles in the simulation down to a 250 eV low-energy limit. The photon cross sections were validated over the energy range between 1 keV and 100 GeV against the NIST reference data (Amako *et al.*, 2005). The simulation has been validated with respect to experimental measurements using EBT2 GafChromic film (International Specialty Products, Wayne, NJ, USA) and a PinPoint 31014 (PTW Freiburg, Freiburg, Germany) ionization chamber (Cornelius *et al.*, 2014).

The energy deposition in the phantom was calculated at the centre of 2 mm $\times$ 0.2 mm $\times$ 0.2 mm scoring voxels for the broad-beam setup and at the centre of 1 mm $\times$ 0.01 mm $\times$ 0.1 mm scoring voxels in the microbeam configuration. The total energy deposited in keV in each voxel was converted to dose in Gy deposited for analysis post-simulation.

A cut (threshold of production of secondary particles expressed in range) of 0.01 mm, corresponding to the length of the smallest voxel dimension, was applied within the phantom in order to reduce simulation times. Additionally, particles were stored in a phase space store placed between the MSC and the phantom in order to reuse the incident radiation field when studying phantoms of different materials without needing to generate primary photons and transport through the beamline for each different simulation set-up.

2.3. Analysis of the results

The absolute dose deposited in the phantom per incident photon was calculated in the voxels of the phantom in units of Gray (Gy). The dose within each voxel of the solid phantom (D_p) was compared with the dose in identically sized and positioned voxels in a water phantom of identical dimensions

(D_w). The percentage dose difference ΔD was calculated using the following equation,

$$\Delta D = \frac{D_p - D_w}{D_w} \times 100. \qquad (3)$$

The relative dose distributions were determined by normalizing the depth dose profiles to their respective maximum doses. Likewise, relative lateral dose profiles were produced by normalizing to the maximum dose. The percentage deviation of the relative dose profiles were derived using equation (3).

Uncertainty of dose was calculated by determining the standard error of dose to 99% confidence in each voxel across 100 simulations of identical fluence, but unique random seeds. Uncertainty of ΔD was calculated using standard propagation of the relative error equation.

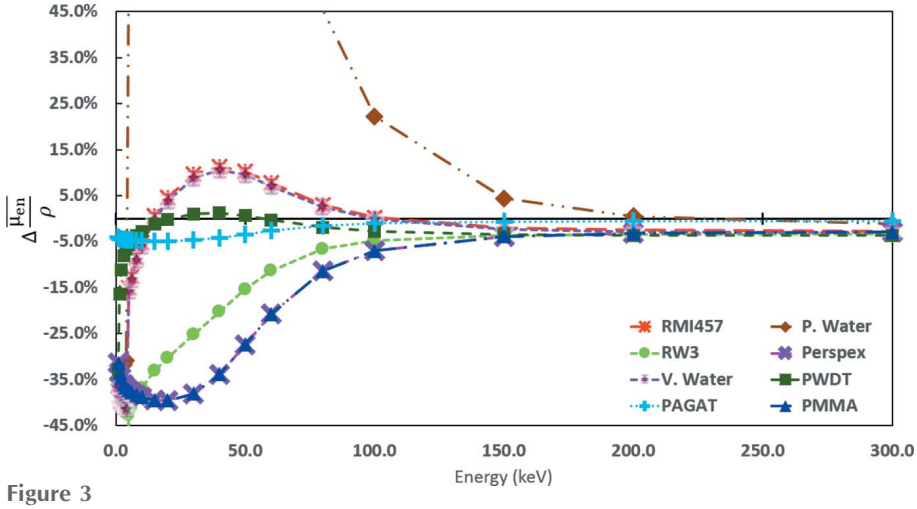

Figure 3
Percentage difference of the mass energy-absorption coefficient $\Delta(\bar{\mu}_{en}/\rho)$ of the solid phantoms under investigation with respect to water, *versus* photon energy.

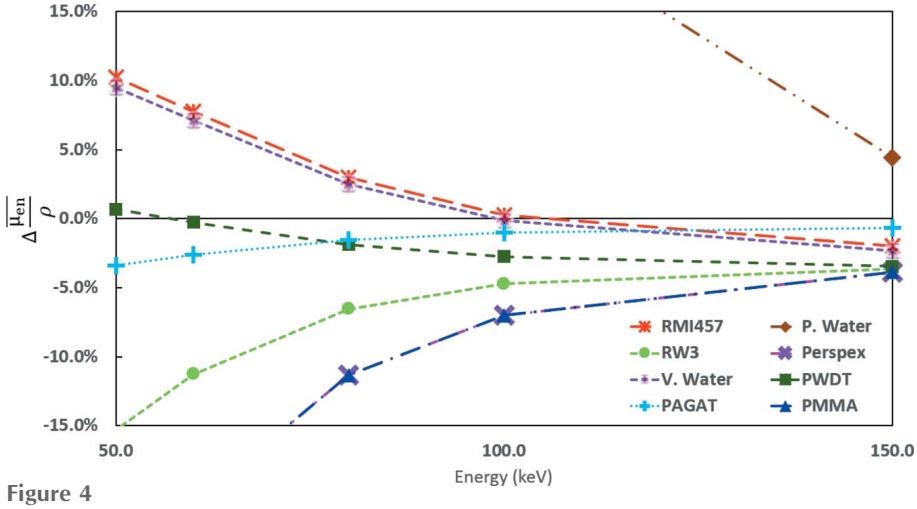

Figure 4
Zoom of Fig. 3 in the photon energy range of interest for MRT (from 50 keV to 150 keV).

3. Results

3.1. Comparison of the mass energy-absorption coefficients of the solid phantoms

Figs. 3 and 4 show the percentage difference of $\bar{\mu}_{en}/\rho$ calculated for all solid phantom materials under study compared with water, in the energy range between 1 keV and 300 keV of interest for MRT. In general, all materials agree with water within 5% for energies higher than ~150 keV, while substantial differences can be observed at low energies (below ~50 keV). $\bar{\mu}_{en}/\rho$ of RMI457 Solid Water and Virtual Water agree within 5–10% with water between 50 keV and 150 keV, which is the energy range of the incident MRT photon beam. RW3 also agrees within 5–10% with water while Plastic Water DT and PAGAT agree within 5% in the same energy range. Thus, RMI457 Solid Water, Virtual Water, Plastic Water DT, PAGAT and RW3 are expected to be the most water-equivalent materials.

Nevertheless, the mass energy-absorption coefficient does not take into account the spatial distribution of the energy deposition, which plays a crucial role in MRT because of the limited sizes of the microbeams. This factor is taken into account in the *Geant4* simulation.

3.2. Broad-beam configuration

Dosimetric results were averaged over appropriately chosen voxels in the centre of the field (CoF) and in a region outside of the field (OoF) to improve statistics. The chosen voxel size for this configuration was 2 mm × 0.2 mm × 0.2 mm and the regions selected for averaging are shown in Fig. 5. The dose was integrated over the selected voxels and then divided by the number of voxels to obtain the average dose in that region. The average dose was then divided by the number of simulated primary photons to obtain the average dose per

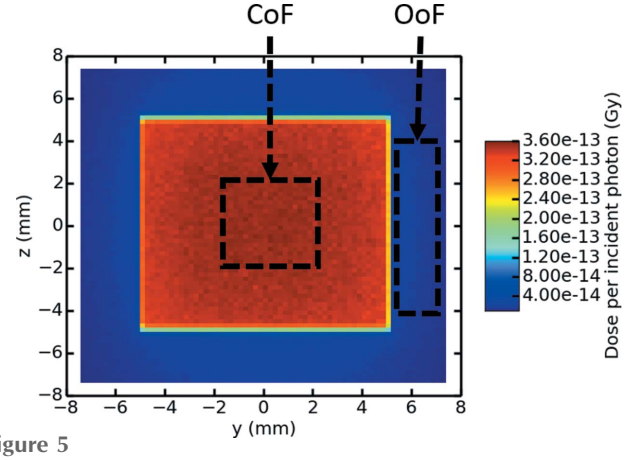

Figure 5
YZ (beam's eye) dose map of the broad-beam configuration showing the CoF and OoF at 2 cm depth.

Table 2
Percentage ΔD [as defined in equation (3)] for the phantom materials under investigation relative to water, in broad-beam configuration for all depths.

The most water-equivalent materials are highlighted in bold face.

Material	CoF	OoF
RMI457 Solid Water	**±1%**	**+5% to −2%**
RW3	−5% to −6%	−7% to −10%
PMMA	−8% to <−20%	−1% to <−20%
Plastic Water DT	**−2% to −4%**	**−1% to −5%**
PAGAT	−1% to −6%	**0% to −5%**
Virtual Water	**±1%**	**+4% to −4%**
Perspex	−8% to <−20%	−1% to <−20%
Plastic Water	+9% to >+20%	>+16%

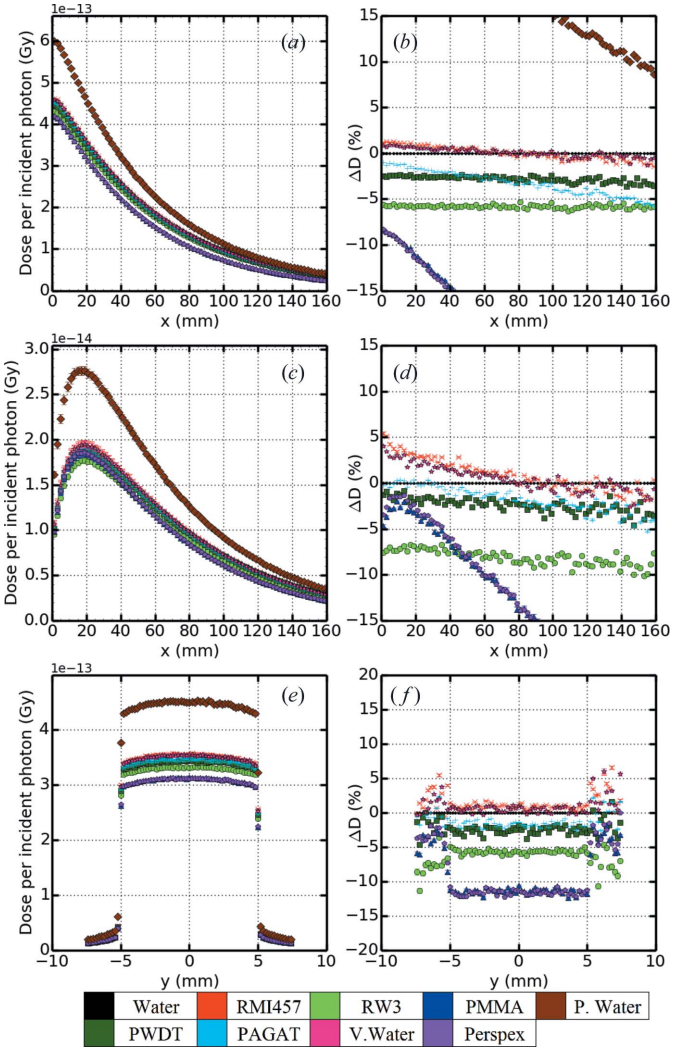

Figure 6
(*a*) Depth dose profile at the centre of field (CoF). (*b*) Percentage ΔD in (*a*) relative to that in water. (*c*) Depth dose profiles out of field (OoF). (*d*) Percentage ΔD in (*c*) relative to that in water. (*e*) Horizontal (*y*) dose profile at 2 cm depth. (*f*) Percentage ΔD in (*e*) relative to that in water. Percentage ΔD is defined in equation (3).

incident photon deposited in the phantom. This methodology is acceptable in regions without steep dose gradients.

Absolute dose distributions, in broad-beam configuration, for all phantom materials under investigation are shown in Fig. 6 and summarized in Table 2. Normalized dose distributions for this configuration are shown in Fig. 7 and summarized in Table 3.

Table 3
Deviation of the relative dose distribution in phantom materials relative to water, as defined in equation (3), in broad-beam configuration for all depths.

The most water-equivalent materials are highlighted in bold face.

Material	CoF	OoF
RW3	**0% to −1%**	**0% to −3%**
PMMA	0% to <−20%	+1% to <−20%
PAGAT	**0% to −5%**	+1% to −6%
Perspex	0% to <−20%	+1% to <−20%
Plastic Water	0% to −17%	+8% to <−20%

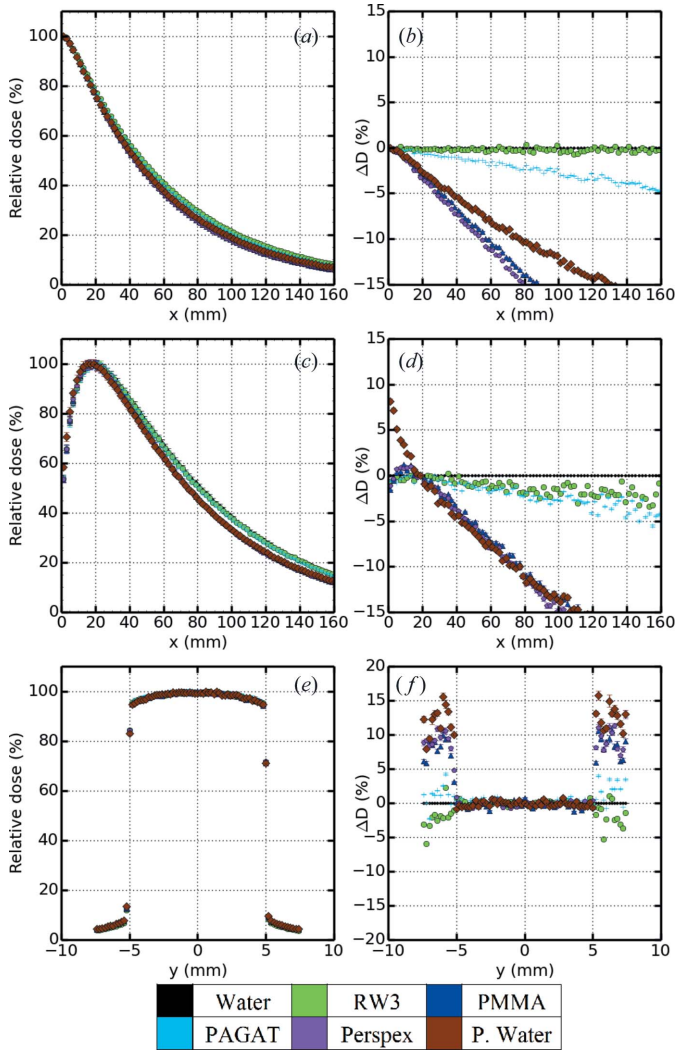

Figure 7
(*a*) Depth dose curve at the centre of field (CoF). (*b*) Percentage ΔD in (*a*) relative to water. (*c*) Depth dose curves out of field (OoF). (*d*) Percentage ΔD in (*c*) relative to water. (*e*) Horizontal (*y*) dose profile at 2 cm depth. (*f*) Percentage ΔD in (*e*) relative to water.

Simulation results for the broad-beam configuration were obtained for an incident photon fluence of 6.2×10^6 mm^{-2} for each phantom material. The statistical uncertainty of the dose

was calculated to be less than 0.8% across all depths at the CoF and less than 2.4% in the OoF region. In this work, adequate agreement between phantom material and water is defined to be within 5% ΔD as in Hugtenburg *et al.* (2010).

The phantom materials providing best agreement with water in the CoF are RMI457 Solid Water and Virtual Water within $\pm 1\%$ ΔD and Plastic Water DT within 4% ΔD [see Figs. 6(*a*) and 6(*b*)].

None of the other phantom materials agree with water for the full depth of the 20 cm $\times$ 30 cm $\times$ 30 cm phantom, but it should be noted that PAGAT fails by only 1% ΔD and RW3 consistently receives doses that are less than water, but that vary only slightly with depth. These results suggest that RW3, PAGAT and Plastic Water DT can be used as phantom materials provided the application of a suitable normalization factor.

PMMA, Plastic Water and Perspex are clearly unsuitable for absolute dosimetry in the CoF as they show significant disagreement.

Virtual Water provides best agreement with water in the OoF region within 4% ΔD, and RMI457 Solid Water and Plastic Water DT provide good agreement within 5% ΔD, as shown in Figs. 6(*c*) and 6(*d*). In addition, PAGAT approximates water within 5% ΔD for all depths considered and thus is a good substitute for water in the OoF region only. It should be noted that ΔD varies more in the OoF region compared with in the CoF region for all the solid phantoms [shown better in Figs. 6(*e*) and 6(*f*)].

Figs. 6(*e*) and 6(*f*) show the horizontal (y) profile of dose in the different phantoms at a depth of 2 cm, which corresponds to a maximum dose in the OoF. While ΔD is relatively constant across the beam in the CoF at this depth, the deviation of the dose is subject to greater variation in the OoF region [as noted above in Figs. 6(*c*) and 6(*d*)]. This is due to the dose in the OoF region being orders of magnitude lower than the dose in the CoF, thus small variations in absolute dose in the OoF region translate to relatively larger differences from water than would occur in the CoF.

This can be seen with RMI457 Solid Water, which shows agreement with water in the broad-beam set-up within $\pm 1\%$ ΔD in the CoF, but in the penumbra the range increases to +5% to -2% ΔD.

Figs. 7(*a*) and 7(*b*) show the relative dose distribution, normalized to the maximum dose as in Hill *et al.* (2010), which has been adopted as a reference to compare our results with. Note that RMI457 Solid Water, Plastic Water DT and Virtual Water were not considered for comparison of relative dose as they had already been shown to agree in the absolute dose case.

When comparing the relative dose distributions, PAGAT and RW3 agree within 5% ΔD in the CoF. This agreement was expected due to the relatively constant -5% ΔD of RW3 across all depths and the fact that PAGAT only exceeded the agreement threshold by 1% in the absolute case. RW3 in particular agrees very well within 1% ΔD. Plastic Water, Perspex and PMMA still do not describe the relative dose distribution of water with adequate accuracy.

Figs. 7(*b*) and 7(*c*) show the normalized depth dose profiles in the OoF. RW3 agrees very well with water in the OoF (within 3% ΔD, the best agreement achieved in OoF) but PAGAT fails to agree in the OoF due to a maximum 6% ΔD. The remaining materials do not agree with water in either the CoF or OoF.

3.3. Microbeam configuration

As in the broad-beam case, results were averaged over appropriately chosen voxels to improve statistics. The voxel size used here was 1 mm $\times$ 0.01 mm $\times$ 0.1 mm, which is smaller than in the broad-beam case to account for the steeper dose gradients in the y-direction. The regions chosen for averaging are shown in Fig. 8. Absolute dose distributions for the microbeam configuration are shown in Fig. 9 and summarized in Table 4. Relative dose distributions for this configuration are shown in Fig. 10 and summarized in Table 5. Dose was recorded both at the central peak and in the valley adjacent to the central peak (see Fig. 8).

Simulations with microbeams were obtained with an incident photon fluence of 3.6×10^7 mm^{-2} for each phantom material. Doses delivered were lower and uncertainties higher despite the larger fluence because the voxel cross-sectional area in the yz plane is 1/40 of the size of the broad-beam case. Statistical uncertainty across all depths was calculated to be less than 2% in the peak and less than 2.3% in the valley.

Given the current lack of dosimetric standards specifically designed for MRT, in this work adequate agreement with water was decided to be within 5% ΔD in the peak where conditions are similar to the broad-beam case. Within the valley the absolute dose is lower, thus smaller variations in dose can result in significant deviations when compared with water. It is therefore reasonable to modify the criteria for agreement when considering valley regions. The criteria for good agreement were relaxed slightly to within 6% ΔD. This is justified by results from Cornelius *et al.* (2014) and Bräuer-Krisch *et al.* (2010) where experimental measurement of dose in the peak using GafChromic film had relative errors of up to approximately 15% and 8%, respectively.

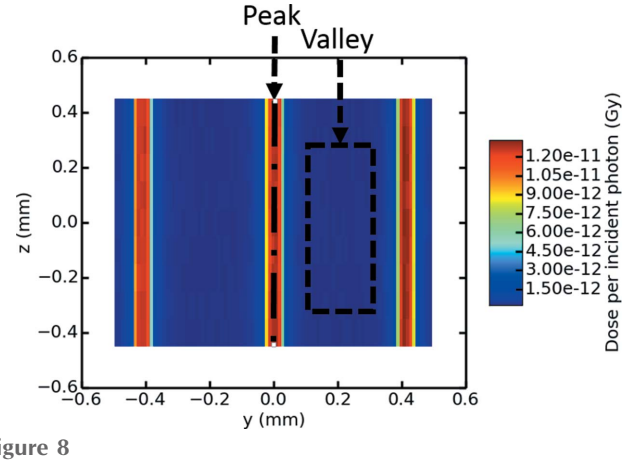

Figure 8
YZ (beam's eye) dose map of the microbeam configuration showing peak and valley regions (in black) at 2 cm depth.

Table 4
Percentage ΔD of phantom materials relative to water, as defined in equation (3), in microbeam configuration for all depths.

The most water-equivalent materials are highlighted in bold face.

Material	Peak	Valley
RMI457 Solid Water	**0% to −3%**	**+6% to −5%**
RW3	−3% to −7%	−8% to −14%
Plastic Water DT	**−2% to −5%**	−1% to −7%
PAGAT	−1% to −7%	0% to −8%
Virtual Water	**0% to −3%**	**+6% to −5%**

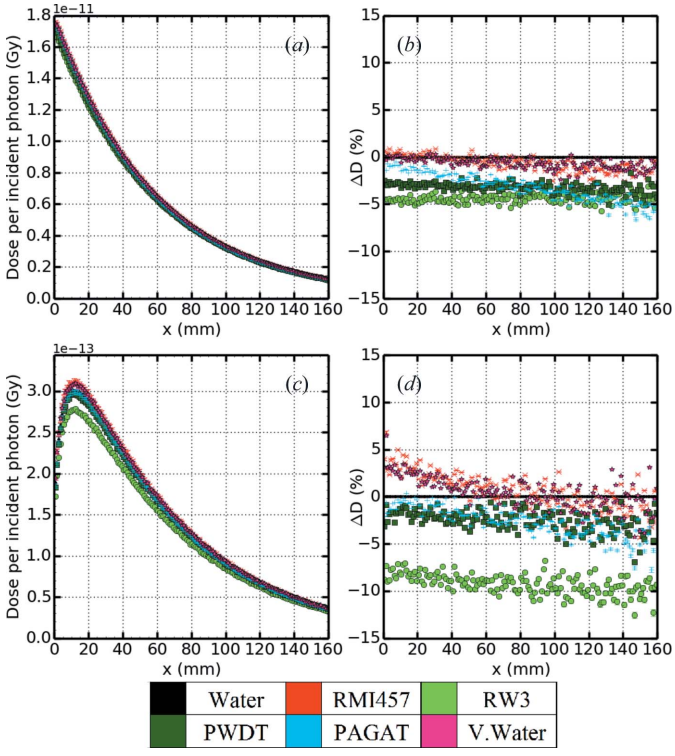

Figure 9
(*a*) Depth dose curve at the peak. (*b*) Percentage ΔD in (*a*) relative to water. (*c*) Depth dose curve in the valley. (*d*) Percentage ΔD in (*c*) relative to water.

Table 5
Percentage ΔD, calculated from normalized dose of phantom materials relative to water, as defined in equation (3), in microbeam configuration for all depths.

The most water-equivalent materials are highlighted in bold face.

Material	Peak	Valley
RW3	**+ 2% to −1%**	**+1% to −5%**
Plastic Water DT	**0% to −3%**	**+1% to −5%**
PAGAT	0% to −7%	+1% to −7%

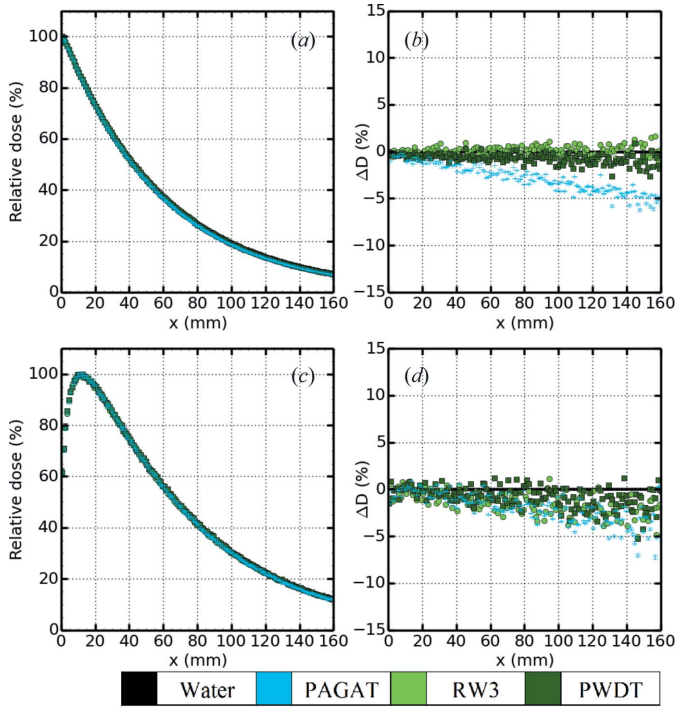

Figure 10
(*a*) Depth dose curve at the peak. (*b*) Deviation of dose in (*a*) relative to that in water. (*c*) Depth dose curve in the valley. (*d*) Deviation of dose in (*c*) relative to that in water.

Materials that did not agree with water at all in the broad-beam case (Perspex, Plastic Water and PMMA) were not considered for the microbeam case in order to reduce simulation times.

The results for the MRT case are shown in Figs. 9(*a*) and 9(*b*). In agreement with the results obtained in the broad-beam configuration, the RMI457 Solid Water and Virtual Water materials best approximate the absolute dose in a water phantom in the peak region with a maximum ΔD of 3% and Plastic Water DT agrees within 5% ΔD.

RW3 and PAGAT do not agree with water in the peak in terms of absolute dose.

The valley dose profiles are shown in Figs. 9(*c*) and 9(*d*). In this case, the phantom materials show substantial differences with respect to water in terms of dose. RMI457 Solid Water and Virtual Water agree within 6% ΔD but span the entire range of +6% to −5% ΔD. RW3, Plastic Water DT and PAGAT do not agree within 6% ΔD, though Plastic Water DT fails by only 1%. RW3 and PAGAT also have a smaller range of deviation than RMI457 Solid Water and Virtual Water, which suggests usefulness for relative dose distribution measurements. Thus, only RMI457 Solid Water and Virtual Water are considered to be in good agreement with water (within 6% ΔD) for microbeam dosimetry QA.

The observed dosimetric differences between peak and valley can be attributed to two facts: firstly that energy deposited in the valley is due to scattered photons and secondly that the dose is two orders of magnitude less than in the peak.

The results indicate that it is difficult to accurately determine a dose relative to water in any phantom material in the valleys. The best relative dosimetric agreement between the considered solid phantoms and water in the OoF is within 6% ΔD. This fact has to be taken into account when determining the PVDRs in water from measurements performed in the investigated solid phantoms, provided that the position of the peak is known.

The normalized microbeam peak profiles are shown in Figs. 10(*a*) and 10(*b*). Once again, materials that agreed in the absolute dose case were not considered when calculating relative dose distributions. As in the broad-beam case, RW3 agrees with water in the peak within 5% ΔD once the dose is normalized, as does Plastic Water DT, but PAGAT fails to agree within 5% ΔD. Figs. 10(*c*) and 10(*d*) show the same trend, RW3 and Plastic Water DT agreeing within 6% ΔD and Plastic Water DT failing by 1%. RW3 and Plastic Water DT both agree within stated limits and thus both materials are recommended for use in QA of MRT relative dosimetry.

4. Discussion

Summarizing the results of our simulation study, RMI457 Solid Water, RW3, Plastic Water DT and Virtual Water are suggested as substitutes for water for MRT QA in the MRT broad-beam configuration. For the MRT microbeam configuration, RMI457 Solid Water and Virtual Water can be used for absolute dosimetry, while RW3 and Plastic Water DT can be used for relative dosimetry only. An approximate normalization factor for the relative dosimetry of microbeams using RW3 would be 1.05 ± 0.15 for the peak and 1.10 ± 0.15 for the valley regions. In the case of the broad-beam configuration, the normalization factor is approximately 1.06 ± 0.05 for the same material.

In the first stage of the study, mass energy-absorption coefficients $\bar{\mu}_{\rm en}/\rho$ were calculated for all the solid phantoms in the photon energy range of interest for MRT. Generally, the materials that were shown to agree in our simulation study (PAGAT, Plastic Water DT, RMI457 Solid Water, RW3 and Virtual Water) also had mass energy-absorption coefficients that were within a few percent of those of water in the energy range of interest. It was found that the materials with the smallest deviation of $\bar{\mu}_{\rm en}/\rho$ from that of water had better dosimetric agreement. Likewise, the materials which were shown to be less water-equivalent from a dosimetric perspective (PMMA, Perspex and Plastic Water) had $\bar{\mu}_{\rm en}/\rho$ values that differed by more than 20% from those of water in the range of interest.

The energy dependence of $\bar{\mu}_{\rm en}/\rho$ necessitates knowledge of the incident energy spectrum in order to select the most appropriate phantom material. Some manufacturers provide a recommended range of energies through which their phantom is most water-equivalent. Plastic Water from CIRS is recommended for the 150 keV to 100 MeV energy ranges, and Plastic Water DT is recommended from 50 keV to 15 MeV. Similarly, PTW Freiburg recommends RW3 for photon energy ranges from ^{60}Co (1.17 and 1.33 MeV) up to 25 MeV. The results obtained in this work for these particular phantoms support the recommendation of the manufacturers. However, this information is not provided by the respective manufacturers for the rest of the phantom materials investigated in this work.

Of particular note is PAGAT, which did not follow the observed correlation between $\bar{\mu}_{\rm en}/\rho$ and dosimetric water equivalence, especially in the microbeam configuration case. A better dose agreement was expected for PAGAT in the absolute dose case, given that $\bar{\mu}_{\rm en}/\rho$ deviated the least from water. This discrepancy can be explained by the observation that the vast majority of deposited energy in the phantom materials is due to Compton scattering, which is dominant from an energy of ~40 keV, and that $\bar{\mu}_{\rm en}/\rho$ does not take into account the backscatter or scattering from distant parts of the radiation field. In larger fields, typical of conventional radiotherapy, the contribution from scatter is less significant than in the case of small field sizes of MRT. This is especially true within the valleys, where the dose is almost entirely due to scattered photons from distant peaks. Our results indicate that $\bar{\mu}_{\rm en}/\rho$ is not sufficient to accurately estimate the water-equivalence of phantom materials in such small radiation fields.

Our results agree with Hill *et al.* (2010) but the exact magnitude of the relative difference of materials from water differs. In both studies, RMI457 Solid Water, Virtual Water, Plastic Water DT, RW3 and PAGAT were all found to be water-equivalent, whilst Perspex, PMMA and Plastic Water were not. Disagreements between the exact magnitude of relative differences of the materials of the two studies (from 2% to 20% depending on the material in question) may be accounted for by noting that our broad-beam results were simulated using a smaller field size (1 cm^2 field as opposed to 2 cm^2) and smaller voxels (2 mm × 0.2 mm × 0.2 mm rectangular prisms as opposed to 10 mm-diameter, 2 mm-thick cylindrical voxels). Differences also arise due to the fact that our results were simulated using a different X-ray energy spectrum (a ~300 keV maximum/~100 keV mean MRT X-ray spectrum as opposed to spectra typical of kV treatment, a ~280 keV maximum/~93 keV mean).

In our study, the dose was calculated in a phantom to a depth of 16 cm along the direction of incidence of the beam as opposed to 6 cm as in Hill *et al.* (2010). We found that agreement with water was better for all phantom materials considered at smaller depths, so some materials that have failed for the 16 cm depth in our 20 cm phantom may provide sufficient agreement at shallower depths and/or in smaller phantoms. With a more relaxed condition for agreement (*e.g.* 8% ΔD in MRT peak and 10% ΔD in the valley), Plastic Water DT and PAGAT may be considered for QA dosimetry even in the absolute dose case, while a stricter condition for agreement may see no materials deemed suitable. More complex phantoms such as bone or anatomical phantoms have yet to be investigated under these conditions and will be the subject of further testing.

Our simulation study shows that phantom materials that agreed in the broad-beam case may not be adequate in the MRT case (specifically PAGAT). Dosimetry within the valley was found to be more difficult and required averaging in order to produce acceptable statistics. This is most evident in the case of RMI457 Solid Water and Virtual Water (when normalized) where doses agreed within the peak but not in the valley. Thus, this study shows that the spatial fractionation has a significant dosimetric effect in phantoms, which cannot be neglected when performing QA studies for MRT.

This work demonstrated that the choice of solid phantom material for QA of MRT must be considered carefully. Moreover, the chosen phantom must be tested to ensure that it is truly water-equivalent in synchrotron beam conditions before use (for example, by comparison of PinPoint ion chamber readings at equivalent depths in water and solid phantoms).

5. Conclusion

In this study, the dose deposition from synchrotron X-rays produced at the ESRF ID17 beamline was simulated in multiple common phantom materials for broad-beam and microbeam MRT configurations using Monte Carlo techniques. Alternative phantom materials were compared against water in terms of dose and the most water-equivalent solid phantom material was determined under simulated conditions.

Based on the results of this study, the adoption of Virtual Water, Plastic Water DT, RW3 and RMI457 Solid Water are recommended for MRT QA as water-equivalent solid phantom materials. In particular, Virtual Water and RMI457 Solid Water agree with water within $\pm 3\%$ relative difference to water in the peak and 6% in the valley and are recommended for absolute dosimetry. RW3 and Plastic Water DT agree within $\pm 3\%$ relative difference to water in the peak and 5% in the valley once normalized and are recommended for relative dosimetry once normalized. Plastic Water DT can also be used in broad-beam QA for absolute dosimetry studies. PMMA, Plastic Water, PAGAT and Perspex are not recommended to be used in relative or absolute dosimetry in MRT.

Acknowledgements

This research was supported by an Australian Government Research Training Program (RTP) Scholarship and the NH&MRC. This work was supported by the Multi-modal Australian ScienceS Imaging and Visualization Environment (MASSIVE) (http://www.massive.org.au). We would like to thank the University of Wollongong Information Management and Technology Services (IMTS) for computing time on the UOW High Performance Computing Cluster.

Funding information

Funding for this research was provided by: National Health and Medical Research Council (award No. Development grant APP1093256).

References

Agostinelli, S. *et al.* (2003). *Nucl. Instrum. Methods Phys. Res. A*, **506**, 250–303.

Allison, J. *et al.* (2006). *IEEE Trans. Nucl. Sci.* **53**, 270–278.

Allison, J. *et al.* (2016). *Nucl. Instrum. Methods Phys. Res. A*, **835**, 186–225.

Amako, K., Guatelli, S., Ivanchenko, V. N., Maire, M., Mascialino, B., Murakami, K., Nieminen, P., Pandola, L., Parlati, S., Pia, M. G., Piergentili, M., Sasaki, T. & Urban, L. (2005). *IEEE Trans. Nucl. Sci.* **52**, 910–918.

Andreo, P., Burns, D. T., Hohlfield, K., Huq, M. S., Kanai, T., Laitano, F., Smyth, V. & Vynckier, S. (2000). *Absorbed dose determination in external beam radiotherapy, an international code of practice for.* IAEA Technical reports series No. 398. Vienna: International Atomic Energy Agency.

Andreo, P., Cramb, J., Fraass, B. A., Ionescu-Farea, F., Izewska, J., Levin, V., Mijnheer, B., Rosenwald, J.-C., Scalliet, P., Shortt, K. R., Van Dyke, J. & Vatnitsky, S. (2004). *Commissioning and quality assurance of computerised planning systems for radiation treatment of cancer*, IAEA Technical reports series No. 430. Vienna: International Atomic Energy Agency.

Attix, F. H. (1984). *Phys. Med. Biol.* **29**, 869–871.

Bartzsch, S. (2011). Master's Thesis. German Cancer Research Center (DKFZ), Germany.

Bartzsch, S., Lerch, M., Petasecca, M., Bräuer-Krisch, E. & Oelfke, U. (2014). *Med. Phys.* **41**, 041703.

Berger, M., Coursey, J., Zucker, M. & Chang, J. (1998). *Stopping power and range tables for electrons, protons and helium ions.* National Institute of Standards and Technology, Gaithersburg, MD, USA.

Bräuer-Krisch, E., Serduc, R., Siegbahn, E. A., Le Duc, G., Prezado, Y., Bravin, A., Blattmann, H. & Laissue, J. A. (2010). *Mutat. Res.* **704**, 160–166.

Bravin, A., Olko, P., Schültke, E. & Wilkens, J. (2015). *Phys. Med.* **31**, 561–563.

Brown, S., Venning, A., De Deene, Y., Vial, P., Oliver, L., Adamovics, J. & Baldock, C. (2008). *Appl. Radiat. Isot.* **66**, 1970–1974.

Chauvie, S., Guatelli, S., Ivanchenko, V., Longo, F., Mantero, A., Mascialino, B., Nieminen, P., Pandola, L., Parlati, S., Peralta, L., Pia, M. G., Piergentili, M., Rodrigues, P., Saliceti, S. & Trindade, A. (2004). *IEEE Nucl. Sci. Symp. Conf. Rec.* pp. 1881–1885.

Cornelius, I., Guatelli, S., Fournier, P., Crosbie, J. C., Sanchez del Rio, M., Bräuer-Krisch, E., Rosenfeld, A. & Lerch, M. (2014). *J. Synchrotron Rad.* **21**, 518–528.

Crosbie, J., Svalbe, I., Midgley, S. M., Yagi, N., Rogers, P. A. W. & Lewis, R. A. (2008). *Phys. Med. Biol.* **53**, 6861–6877.

Debus, C. (2012). Masters's thesis, German Cancer Research Center (DKFZ), Germany.

De Felici, M., Felici, R., del Rio, M. S., Ferrero, C., Bacarian, T. & Dilmanian, F. A. (2005). *Med. Phys.* **32**, 2455–2463.

Fernandez-Palomo, C., Bräuer-Krisch, E., Laissue, J., Vukmirovic, D., Blattmann, H., Seymour, C., Schültke, E. & Mothersill, C. (2015). *Phys. Med.* **31**, 584–595.

Fournier, P., Crosbie, J. C., Cornelius, I., Berkvens, P., Donzelli, M., Clavel, A. H., Rosenfeld, A. B., Petasecca, M., Lerch, M. L. F. & Bräuer-Krisch, E. (2016). *Phys. Med. Biol.* **61**, N349–N361.

Hill, R., Brown, S. & Baldock, C. (2008). *Radiat. Meas.* **43**, 1258–1264.

Hill, R., Healy, B., Holloway, L., Kuncic, Z., Thwaites, D. & Baldock, C. (2014). *Phys. Med. Biol.* **59**, R183–R231.

Hill, R., Kuncic, Z. & Baldock, X. (2010). *Med. Phys.* **37**, 4355–4363.

Hubbell, J. H. & Seltzer, S. M. (1993). *Tables of X-ray mass attenuation coefficients from 1 keV to 20 MeV for elements Z = 1 to 92 and 48 additional substances of dosimetric interest*, Table 3. Radiation and Biomolecular Division, National Institute of Standards and Technology, Bethesda, MD, USA.

Hugtenburg, R., Adegunloye, A. & Bradley, D. (2010). *Nucl. Instrum. Methods Phys. Res. A*, **619**, 221–224.

ICRU (1989). *ICRU Technical Report 44.* International Commission on Radiation Units and Measurements, Inc., Bethesda, MD, USA.

Lerch, M. L. F., Dipuglia, A., Cameron, M., Fournier, P., Davis, J., Petasecca, M., Cornelius, I., Perevertaylo, V. & Rosenfeld, A. B. (2017). *J. Phys. Conf. Ser.* **777**, 012009.

Lerch, M., Petasecca, M., Cullen, A., Hamad, A., Requardt, H., Bräuer-Krisch, E., Bravin, A., Perevertaylo, V. L. & Rosenfeld, A. B. (2011). *Radiat. Meas.* **46**, 1560–1565.

Livingston, J., Stevenson, A., Butler, D., Hausermann, D. & Adam, J. (2016). *Med. Phys.* **43**, 4283–4293.
Ortiz, P., Cosset, J. M., Holmberg, O., Rosenwald, J. C., Dunscombe, P., Pinillos, L., Vilaragut, J. J. & Vatnitsky, S. (2009). *Ann. ICRP*, **39**, 1–86.
Petasecca, M., Cullen, A., Fuduli, I., Espinoza, A., Porumb, C., Stanton, C., Aldosari, A. H., Bräuer-Krisch, E., Requardt, H., Bravin, A., Perevertaylo, V., Rosenfeld, A. B. & Lerch, M. L. F. (2012). *J. Instrum.* **7**, P07022.
Rosenfeld, A., Siegbah, E. A., Brauer-Krish, E., Holmes-Siedle, A., Lerch, M. L. F., Bravin, A., Cornelius, I. M., Takacs, G. J., Painuly, N., Nettelback, H. & Kron, T. (2005). *IEEE Trans. Nucl. Sci.* **52**, 2562–2569.
Rothkamm, K., Crosbie, J., Daley, F., Bourne, S., Barber, P., Vojnovic, B., Cann, L. & Rogers, P. (2012). *PLoS One*, **7**, e29853.
Sanchez del Rio, M., Canestrari, N., Jiang, F. & Cerrina, F. (2011). *J. Synchrotron Rad.* **18**, 708–716.
Schültke, E., Juurlink, B. H. J., Ataelmannan, K., Laissue, J., Blattmann, H., Bräuer-Krisch, E., Bravin, A., Minczewska, J., Crosbie, J., Taherian, H., Frangou, E., Wysokinsky, T., Chapman, L. D., Griebel, R. & Fourney, D. (2008). *Eur. J. Radiol.* **68**, S142–S146.
Siegbahn, E., Stepanek, J., Bräuer-Krisch, E. & Bravin, A. (2006). *Med. Phys.* **33**, 3248–3259.
Svensson, G. K., Baily, N. A., Loevinger, R., Morton, R. J., Moyer, R. F., Purdy, J. A., Shalek, R. J., Woolton, P. & Wright, K. A. (1994). *AAPM Report No. 13: Physical Aspects of Quality Assurance in Radiation Therapy*. New York: American Institue of Physics.
Zeman, W., Curtis, H., Gebhard, E. & Haymaker, W. (1959). *Science*, **130**, 1760–1761.